scientific reports

Check for updates

OPEN

A high precision vital signs detection method based on millimeter wave radar

Yuanchang Chen, Jiangnan Yuan✉ & Jun Tang

Millimeter wave (mmWave) radar technology has potential applications in vital signs detection and medicine. In order to minimize the influence of human micro-movements and respiratory harmonics on heart rate estimation, the vital signs detection method based on mmWave radar is studied in this paper. First, we use median filtering to eliminate baseline drift caused by human micromotion. Next, a differential recursive least squares multiple classification (DR-MUSIC) algorithm is proposed based on the combination of recursive least squares-based adaptive filter (RLS) and multiple signal classification (MUSIC) algorithm. This algorithm effectively suppresses respiratory harmonics and separates respiratory and heartbeat signals. Finally, heart rate value can be precisely estimated using spectral peak search. We invite a number of people to participate in the experiment, which demonstrate that the method successfully suppresse the impact of respiratory harmonics at low SNR. The error rate between the estimated heart rate and the reference heart rate is only 1.69% to 2.61%, which is significantly better than the existing algorithms.

In recent years, there has been a revolution in the field of vital signs detection due to rapid advances in science and technology and growing public interest in health monitoring. This has resulted in several research breakthroughs. Monitoring of heartbeat and respiration are particularly critical and are important indicators for assessing health status[1–3]. The medical field has traditionally relied on contact monitoring techniques, such as photoplethysmography (PPG)[4] and electrocardiography (ECG)[5]. However, these methods may cause additional risk or discomfort when used in certain patient populations, such as burn victims. To address this challenge, non-contact mmwave radar technology has emerged and received much attention for its advantages in sensitivity and non-invasiveness[6–10].

Frequency modulated continuous wave (FMCW) radars have been successful in non-contact vital signs detection[11–13] due to their excellent range resolution[14], compact size, and low power consumption[15]. These characteristics make FMCW radar not only provide an efficient alternative to existing medical monitoring methods and open up new possibilities in the field of medical and health monitoring. Examples of applications include monitoring human sleep[16,17] and tracking infant health[18,19].

In recent decades, mmwave radar technology has significantly improved the precision of detecting vital signs[20–23]. Specifically, scholars have developed numerous innovative methods to enhance the precision of heart rate estimation. For example, Lin et al[24] successfully reduced respiratory harmonics interference by reconstructing the respiratory signal, resulting in a 3.2% reduction in heart rate estimation error. Hang et al[25] proposed using an adaptive harmonic comb trap digital filter to eliminate respiratory harmonic interference without affecting the heartbeat signal. However, the use of the time-window variation technique[26] to detect vital signs increased the uncertainty of detecting the peak heartbeat signal and resulted in a heart rate error rate exceeding 3.2%. Hu et al[27] integrated both the empirical mode decomposition (EMD) and continuous wavelet transform (CWT) techniques. However, this method resulted in heart rate errors ranging from 2.53% to 4.83% despite its effectiveness in high SNR scenarios. Duan et al[28] used the variational modal decomposition (VMD) technique to determine heart rate, but the margin of error for the heart rate was over 10%. Recently, Ling et al[29] recently introduced a combination of Adaptive Nodal Filter (ANF) and Empirical Wavelet Transform (EWT) to separate heartbeat signals.

Although previous studies have provided a foundation for measuring heartbeat signals, they still fall short in terms of accuracy. In this paper, we propose a high precise vital signs detection method based on mmWave radar technology, designed to overcome existing limitations. The contributions of this paper are:

School of Optoelectronic and Communication Engineering, Xiamen University of Technology, Xiamen 361000, China. ✉email: jnyuan@xmut.edu.cn

1. Application of median filtering: by applying the median filtering technique, we successfully eliminate the baseline drift in the echo signal and effectively avoid possible aberrations in the subsequent spectral estimation process, such as spikes in the low-frequency component. This has results in improved measurement accuracy.
2. Design of DR-MUSIC algorithm: to address the issue of interference from respiratory harmonics on heart rate estimation, we propose a differential recursive least squares multiple classification (DR-MUSIC) algorithm that combines recursive least squares and multiple signal classification algorithms[30]. The algorithm effectively suppresses respiratory harmonics in a low SNR environment and amplifies the heartbeat signal. The function for high resolution spectral estimation is used to locate the target signal, resulting in a notable enhancement in the precision of heart rate measurement. Furthermore, the DR-MUSIC algorithm is more memory-efficient and practical.The rest paper are organized as follows: Section II provides a comprehensive analysis of the fundamental operational principles of the FMCW radar and outlines its potential employment in the detection of vital signs. In Section III, we describe in detail the complete signal processing flow for vital sign detection, including the implementation of the median filtering and the DR-MUSIC algorithm. Section IV demonstrates the significant improvement of our method in accurately estimating heart rate through actual measurement of mmWave radar. Finally, Section V summarizes the research findings and discusses the limitations of the methodology, and provides suggestions for future research directions.

Principle for detecting vital signs based on FMCW radar

In this paper, we use the Texas Instruments (TI) IWR1443BOOST radar sensor, which operates in the 77-81 GHz frequency range. The sensor possesses exceptional measurement precision. Fig 1 shows the system structure.

The fundamental principle of FMCW radar is to emit a continuous electromagnetic wave signal with a frequency that varies over time. When the signal is reflected back to the radar by the target object, it is mixed with the original transmit signal to obtain the IF signal. This signal allows for the accurate calculation of the distance between the target object and the radar, which is crucial for precise heart rate measurement.

The equation for the frequency versus time of a linear FMCW radar during a sweep duration of T_c is as follows:

$$f(t) = f_0 + \mu t = f_0 + \frac{B}{T_c}t. \tag{1}$$

Where f_0 represents the initial frequency of the radar transmission signal, μ represents the FM slope, and B represents the bandwidth of the LFM signal during the duration of the slope. The equation for the angular frequency of the transmitted signal as a function of time is provided by:

$$\omega(t) = 2\pi f(t) = 2\pi(f_0 + \frac{B}{T_c}t). \tag{2}$$

The phase of the signal can be obtained by calculating the integral of the angular frequency. Thus, the instantaneous phase of the transmitted signal can be expressed as:

$$\theta(t) = \int_0^t \omega(\tau)d\tau = 2\pi f_0 t + \pi\frac{B}{T_c}t^2. \tag{3}$$

Thus, the expression for the transmitted signal of the FMCW radar can be obtained as:

$$S_T(t) = A_T \exp\left\{j\left(2\pi f_0 t + \pi\frac{B}{T_c}t^2 + \varphi(t)\right)\right\}. \tag{4}$$

where A_T represents the amplitude of the transmitted signal and $\varphi(t)$ represents the phase noise. When the transmitted signal detects the target object and reflects off it, the reflected signal is received and it can be expressed as:

$$S_R(t) = A_R \exp\left\{j\left(2\pi f_0 (t-\tau) + \pi\frac{B}{T_c}(t-\tau)^2 + \varphi(t-\tau)\right)\right\}. \tag{5}$$

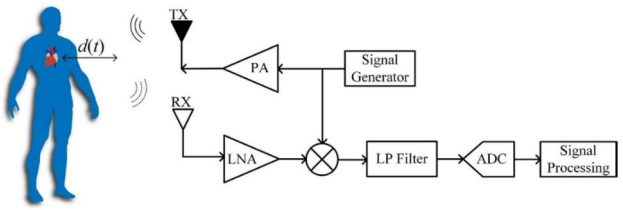

Fig. 1. Block diagram of the radar system.

$$\tau = \frac{2R}{c}. \tag{6}$$

Where τ represents the time delay between the transmitted signal and the received signals, and R represents the distance between the radar and the target. The reflected signal is mixed with the reference signal to obtain the IF signal $\mathrm{S}_{IF}(t)$, which can be expressed as:

$$\mathbf{S}_{IF}(t) = A_{IF} \exp\left\{ j\left(2\pi \frac{B}{T_c}\tau t + 2\pi f_0 \tau - \pi \frac{B}{T_c}\tau^2 + \Delta\varphi(t) \right) \right\}. \tag{7}$$

Where A_{IF} represents the amplitude of the IF signal and $\Delta\boldsymbol{\varphi}(t)$ represents the phase noise. The periodic undulating motion of the body surface caused by respiration and heartbeat is $x(t)$, which can be obtained by organizing the carryover into the IF signal expression $\tau = \frac{2[d_0+x(t)]}{c}$.

$$\begin{aligned} \mathbf{S}_{IF}(t) &= A_{IF} \exp\left\{ j\left(\frac{4\pi B d_0}{cT_c} t + \frac{4\pi\left[d_0 + x(t)\right]}{\lambda_0} \right) \right\} \\ &= A_{IF} \exp\left[j\left(2\pi f_b t + \varphi_b(t) \right) \right] \end{aligned} \tag{8}$$

where the $x(t)$ in $\varphi_b(t)$ implies information about the rise and fall of the chest cavity caused during human physiological activity. The IF signal is sampled in the fast and slow time dimensions, respectively. The echo signal of the m Chirp and the n sampling point can be expressed after ADC processing:

$$S_{IF}[n,m] = A_{IF} \exp\left\{ j\left[\frac{4\pi B d_0}{cT_c} n T_f + \frac{4\pi[d_0 + x(mT)]}{\lambda_0} \right] \right\}. \tag{9}$$

The IF signal phase includes the distance between the body and antenna d_0, and the periodic rise and fall of the chest $x(mT)$. The changes in thoracic micromotion are displayed in a 2D matrix, as illustrated by the curves in Fig 2.

In this paper, we have successfully determined the distance gate where the target is located using the distance dimensional Fast Fourier Transform . As shown in Fig 2, the orange bars representing human targets and the gray bars revealing the distribution of static clutter. By determining the distance gate index where the human target is located, we can extract phase information from it. This phase information not only reveals the ebb and flow of the chest but also contains critical vital sign information, such as heartbeat information.

Signal processing flow on vital signs detection

Based on the previous discussion of the principle of non contact vital sign detection by FMCW radar, we designe a high precision heart rate estimation system. Its signal processing flowchart is shown in Fig 3:

1. Preprocessing: we preprocess the data by eliminating static clutter from the ADC data. Then, we use distance-dimensional Fast Fourier Transform (FFT) to determine the optimal distance gate.
2. Phase information extraction: an inverse tangent function is used to extract the phase information of the chest vibration signal by implementing phase expansion. Subsequently, the median filtering technique is used to eliminate the baseline drift in the signal, thereby improving the signal quality.

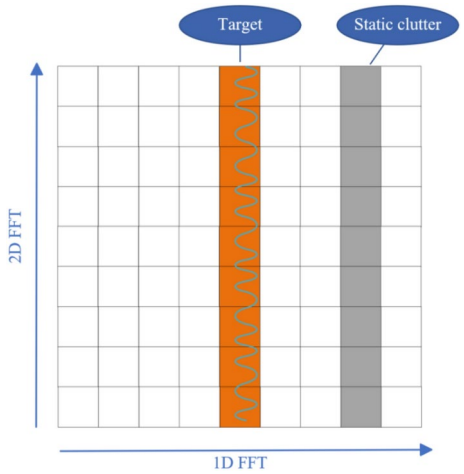

Fig. 2. Schematic representation of thoracic motion in a 2D matrix.

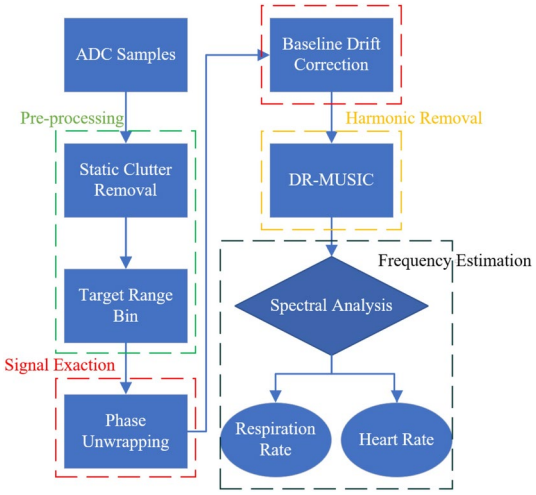

Fig. 3. Signal processing flowchart.

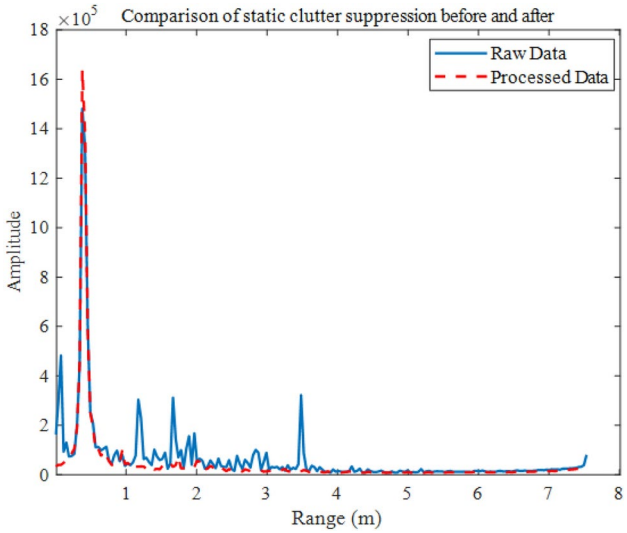

Fig. 4. Comparison of echo signal static clutter removal before and after implementation.

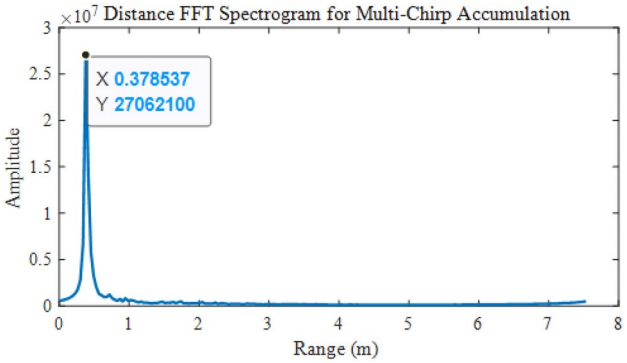

Fig. 5. Distance FFT spectrogram for multi-chirp accumulation.

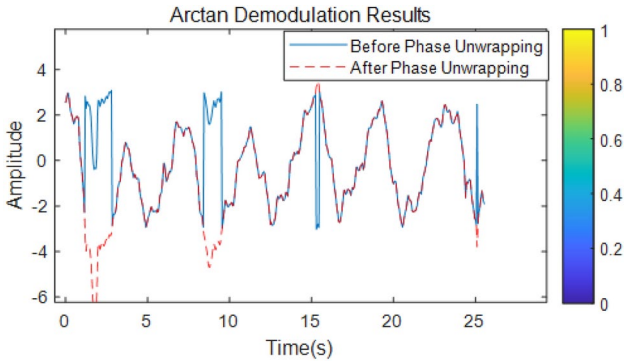

Fig. 6. Arctan demodulation results.

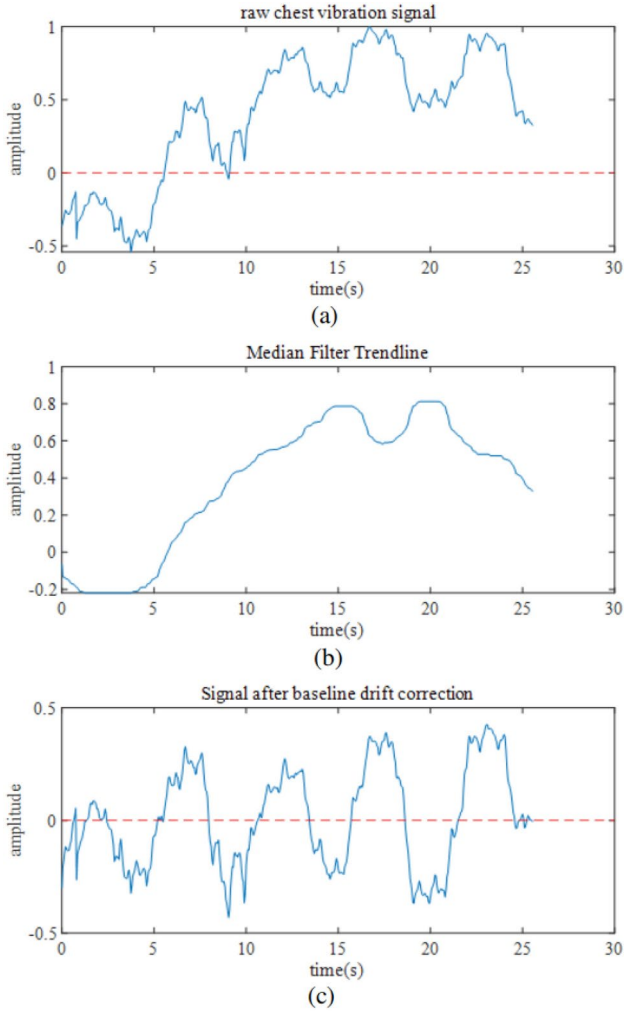

Fig. 7. Plot of median filtering to remove baseline drift results. (a) Raw chest vibration signal. (b) Median filter trendline. (c) Signal after baseline correction.

3. Respiratory harmonics suppression: the design of the DR-MUSIC algorithm is one of the core contributions of this paper. This algorithm effectively suppresses respiratory harmonics interference in a low SNR environment and significantly increases the amplitude of the heartbeat signal.
4. Frequency estimation: the frequency of the heartbeat signal is then estimated using the spectral peak search method.In the following sections, we will discuss these steps in detail.

Echo signal preprocessing

Eliminating static clutter

In the field of mmWave radar signal processing, the challenge of static clutter caused by radar hardware and environmental factors must be addressed. To solve this issue, the phase mean elimination technique is used, which exhibits superior performance in eliminating static clutter. The basic principle of the phase-mean elimination method is to use the property that the distance from a stationary target to a radar antenna is constant. The latency of the stationary target remains constant on each received pulse. By averaging all receive pulses, a reference receive pulse is generated. Then, the difference between each pulse and the reference pulse is calculated. The mathematical expression for this method is as follows:

$$Y(n) = X(n) - \bar{X}. \tag{10}$$

Where $Y(n)$ represents the target echo data after clutter removal, $X(n)$ represents the original target echo data, and $\bar{X}$ represents the mean value of the phase volume.

As shown in Figu 4, the phase mean cancellation method produces remarkable results. It effectively suppresses static clutter in indoor environments while preserving the key features of vital sign signals.

Target unit positioning

The optimal distance gate is determined by accumulating energy after removing static clutter interference. A spectrogram is used to select a specific frequency range and distance gates are used as windows to accumulate signal energy within each window. This produces a series of energy cumulants, each corresponding to a distance gate. The distance gate with the highest cumulative value is selected as the optimal distance gate, which indicates the position of the target. The expression is as follows:

$$X_{acc}[n] = \sum_{k=1}^{M} |X[n,k]|. \tag{11}$$

Fig 5 shows that the distance gate at 0.3785 has the highest cumulative energy. This enables us to precisely locate the distance gate as a human target. By extracting the phase information of this distance gate, we obtain critical data for analyzing vital sign signals.

Target phase information extraction

Phase unwinding

In this paper, we use the inverse tangent function method to extract phase information. By calculating the phase value of each chirp signal at the optimal distance gate location, we can track changes in vital signs over time in detail. The phase variation with time is given by:

$$\phi(t) = \arctan\left[\frac{B_Q(t)}{B_I(t)}\right] = \frac{4\pi x(t)}{\lambda_0} + \varphi_0. \tag{12}$$

Where $B_I(t)$ represents the real component of the complex signal, $B_Q(t)$ represents its imaginary component, and φ_0 represents the phase shift resulting from the fixed distance d_0.

However, this nonlinear operation limits the phase information to a narrow range of ($-\pi$ to π), which restricts the dynamic range. If the phase variation of a signal falls outside of this range, it can result in phase wrapping and prevent the accurate measurement of the phase change. To overcome this challenge, we perform phase unwinding on it. If the difference between adjacent phases exceeds π, the current phase is adjusted by subtracting π. If the phase difference is less than $-\pi$, the correction is made by adding π. If the absolute value of the phase difference is less than π, it indicates that the phase has not changed and remains the same.

As shown in the Fig 6, the initial echo signal displays sudden changes at different points. The phase unwinding operation corrects the phase jumps in the echo signal, resulting in a more coherent phase waveform. This essentially restores the trend of the chest rise and fall.

Baseline drift removal

Even when rest, the echo data shows several trends due to the slight swaying of the limbs. These trend terms can mask important features in the signal and affect the accuracy of the observation. Correcting for baseline drift is critical because both baseline drift and vital sign signals belong to the low-frequency category. This paper introduces a baseline drift removal algorithm based on median filtering specifically designed for correcting baseline drift in vibration signals. The mathematical expression of the algorithm is provided below:

$$y(t) = x(t) - b(t). \tag{13}$$

Where, $x(t)$ represents a thoracic vibration signal containing baseline drift, $b(t)$ represents a trend signal calculated using a median filtering algorithm, and $y(t)$ represents a thoracic vibration signal with baseline drift removed. The steps to solve Trendline $b(t)$ are as follows:

1. Window definition: define a filter window for each data point that includes the current point and its equivalent points before and after. This window should slide from the beginning of the signal to the end to ensure full data coverage.
2. Median value calculation: within each window by arranging the data points in ascending order and selecting the middle value. The median value represents the filtered data points, improving the accuracy of the filtering.
3. Boundary processing: to ensure the integrity of the filtering process and accurate processing of the signal boundary, we use the zero filling method for the signal boundary.
4. Filtering results: finally, we obtain a new signal with the same length as the original signal, which contains all the median filtered data points.

The results presented in Fig 7 demonstrate that median filtering is an effective method for removing the trend term from the original chest vibration signal. This treatment results in a stable signal waveform near the time axis, reducing low-frequency interference caused by slight body oscillations and creating optimal conditions for accurate analysis of vital sign signals.

DR-MUSIC

One significant issue with traditional methods of measuring heart rate is the impact of respiratory harmonic signals on the heartbeat signal, which can significantly affect measurement accuracy. Specifically, respiratory motion generates corresponding respiratory harmonics, which are typically much stronger than the heartbeat signal. As a result, the weaker heartbeat signal is easily masked by these respiratory harmonics, causing confusion between the two frequencies and thereby affecting the accuracy of heartbeat detection. To address this challenge, the DR-MUSIC algorithm is proposed in this paper. This algorithm uses adaptive filtering techniques and integrates phase differencing operations with the MUSIC algorithm. The main benefit of this technique is its capacity to increase the strength of the heartbeat signal while minimizing the impact of respiratory harmonic interference.

To reduce the impact of respiratory harmonics on the heartbeat signal, we design an RLS filter to adaptively cancel the respiratory harmonic noise. The basic principle of the adaptive filter is based on the RLS algorithm, which is shown in Fig 8. In this paper, we use FIR filters instead of IIR filters because FIR filters only require adjustment of their zero parameters, while IIR filters require consideration of both zero and pole parameters as well as filter stability.

Where $U(n)$ represents the chest echo signal that includes the respiratory signal, respiratory harmonics, and heartbeat signal at n moments, $d(n)$ is the reference signal constructed from the fundamental frequency of the respiratory signal at n moments. The difference signal $e(n)$ is obtained by comparing the output signal $y(n)$ with the reference signal $d(n)$. The filter parameters of the filter are continuously adjusted based on the value of $e(n)$ and the adaptive filtering algorithm until the set of filter coefficients becomes smooth. When the filter coefficients converge, the difference $e(n)$ between the input signal and the output signal clearly represents the signal that has been subjected to the adaptive filtering algorithm to remove the respiratory harmonics.

The steps of RLS adaptive filter realization are:

1. Initialization: at time 0, define the values of the FIR filter tap weight vector $W(n)$ and the inverse matrix of the autocorrelation matrix $P(n)$.
2. Recursive ComputingSet n equal to 1 and execute the algorithm steps sequentially:

(1) Update the gain vector $G(n)$:

$$G(n) = \frac{\lambda^{-1}P(n-1)U(n)}{1+\lambda^{-1}U^{\top}(n)P(n-1)U(n)}. \tag{14}$$

(2) Update the filter tap weight vector $W(n)$:

$$W(n) = W(n-1) + G(n)\left[d(n) - U^{\mathrm{T}}(n)W(n-1)\right]. \tag{15}$$

(3) Update the inverse matrix of the autocorrelation matrix $P(n)$:

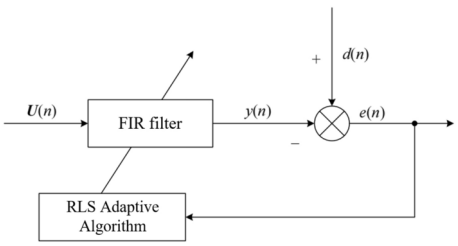

Fig. 8. Schematic diagram of the basic principle of adaptive filter based on RLS algorithm.

$$P(n) = \lambda^{-1}P(n-1) - \lambda^{-1}G(n)U^{\mathrm{T}}(n)P(n-1). \tag{16}$$

(4) Iterate until the estimation error reaches the required level by adding 1 to n and returning to step (1).

Although respiratory harmonics have been effectively eliminated during vital signs processing by using an RLS adaptive filter, detecting the weak heartbeat signal is still a challenge. To improve the detection of heartbeat signals, we introduce the phase difference operation as a crucial step. This method effectively removes the low-frequency portion of the signal by computing the difference between adjacent moments of the signal, which significantly enhances the ability to detect weak signals. The phase-difference operations excel in emphasizing crucial characteristics of a signal, making periodic or frequency-specific components more visible. This processing not only accentuates the faint heartbeat signal but also proficiently attenuates noise. Since noise typically lacks consistent phase characteristics, it is not enhanced during phase differencing. Therefore, this technique results in further enhancement of the SNR and creates better conditions for precise detection of faint heartbeat signals.

By using both RLS adaptive filters and phase-differential operations, we eliminate the respiratory harmonic interference and significantly improve the faint heartbeat signal. To precisely extract the heart rate frequencies from the vital signals, we use the MUSIC algorithm for high accuracy spectral analysis. The implementation of the MUSIC algorithm improves frequency information extraction accuracy and exhibits exceptional signal decomposition performance. In the following section, we describe the implementation steps of the MUSIC algorithm in detail.

After the phase difference operation, the mathematical model can be expressed as:

$$y(n) = \sum_{P=1}^{P} \alpha_P e^{j2\pi f_p n} + w(n). \tag{17}$$

Where, f_p represents the normalized frequency and $w(n)$ represents the Gaussian white noise. Let the value of $y(n)$ be M. The equation can be expressed as follows:

$$y(n) = [y(n)y(n-1)\cdots y(n+M-1)]^T. \tag{18}$$

In our implementation, multiple snapshot signals are obtained by continuously sampling the signal over multiple time intervals. Each snapshot corresponds to a set of complex signal data points collected within a short time period (e.g., a chirp). These snapshots are then used to construct a covariance matrix, enabling the high-resolution spectral analysis of the MUSIC algorithm. The autocorrelation matrix of $y(n)$ is:

$$\begin{aligned} R_x &= E[y(n)y(n)^H] \\ &= \mathrm{Rs} + \mathrm{Rw} \\ &= \sum_{p=1}^{p} |\alpha_p|^2 \nu(f_p)\nu(f_p)^H + R_w \\ &= VAV^H + R_w \end{aligned} \tag{19}$$

The eigenvalues are used to express the autocorrelation matrix:

$$R_x = \sum_{m=1}^{M} \lambda_m \boldsymbol{q}_m \boldsymbol{q}_m{}^H = \boldsymbol{Q}\boldsymbol{\Lambda}\boldsymbol{Q}^H. \tag{20}$$

where λ_m represents the descending order, q_m represents the eigenvector corresponding to the eigenvalue, and Λ represents the diagonal matrix.

The first P eigenvalues represent the signal power:

$$\lambda_m = M|\alpha_m|^2 + \sigma_m^2 (m = 1, 2\cdots, P). \tag{21}$$

The last $P + 1 - M$ eigenvalues are the noise power:

$$\lambda_m = \sigma_m^2 (m = \mathrm{P}+1, \mathrm{P}+2..., \mathrm{M}). \tag{22}$$

The signal space can be divided into two subspaces: the signal subspace and the noise subspace.

$$\begin{aligned} R_x &= (M|\,\alpha_m|^2 + \sigma_m^2) q_m q_m{}^H + \sum_{m=P+1}^{M} \sigma_m^2 q_m q_m{}^H \\ &= Q_s \Lambda_s Q_s^H + Q_w \Lambda_w Q_w^H \end{aligned} \tag{23}$$

Since the signal and noise subspaces are orthogonal, can be expressed by the following equation:

$$v^H(f_p)q_m = \sum_{k=1}^{M} q_m(k)e^{-j2\pi f_p(k-1)} = 0. \tag{24}$$

The frequency spectrum estimation function can be derived from this:

$$R_{phd}(e^{j2\pi f}) = \frac{1}{\sum_{m=P+1}^{M} \frac{1}{\lambda_m}|v^H(f_p)q_m|^2}. \tag{25}$$

By analyzing the peaks in the spectrum, we can accurately estimate the frequency of the heartbeat signals.

To evaluate the performance and effectiveness of the DR-MUSIC algorithm in advance, a series of simulation experiments are being conducted using the MATLAB R2022a software. The frequency sweep range is set to [0Hz, 1.6Hz]. Figure 9 shows a comparison between the waveforms of the signal processed by the DR-MUSIC algorithm and the original signal under varying SNR conditions.

Mmwave radar measurement

Experimental preparation

The experiment use the IWR1443BOOST mmWave radar sensor from Texas Instruments and the DCA1000 EVM data acquisition board as hardware modules. Fig 10 displays the hardware connections. The ADC data is obtained through the mmWave Stdio software provided by Texas Instruments. The radar parameters are configured according to the settings in Tab 1. The data is then transferred to a PC using a USB cable for processing with MATLAB.

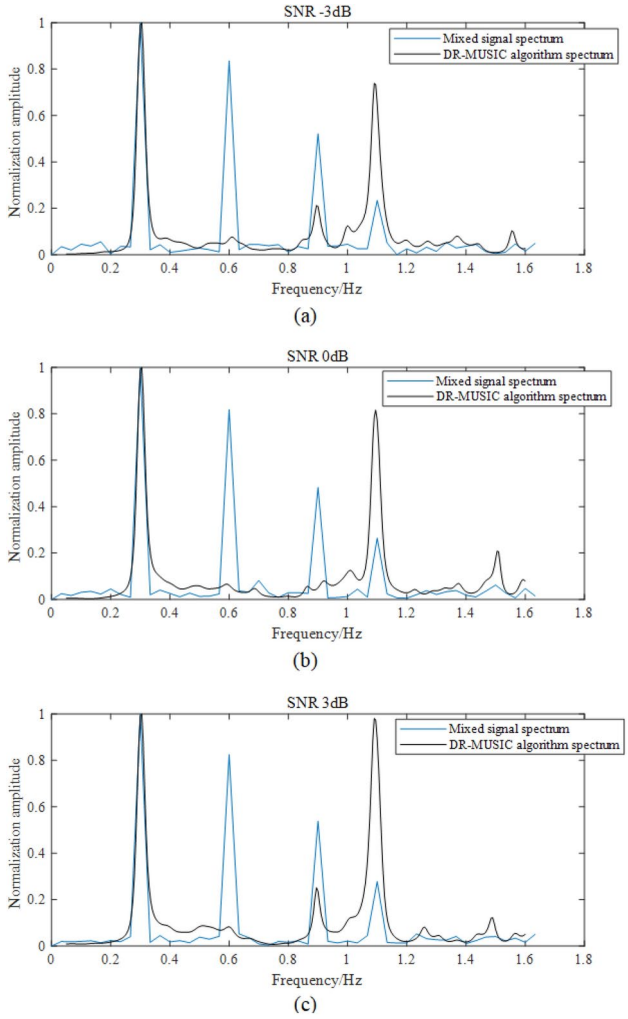

Fig. 9. Comparison of two signal waveforms under different SNR conditions. (a) Comparison of two signal waveforms at -3 dB. (b) Comparison of two signal waveforms at 0 dB. (c) Comparison of two signal waveforms at 3 dB.

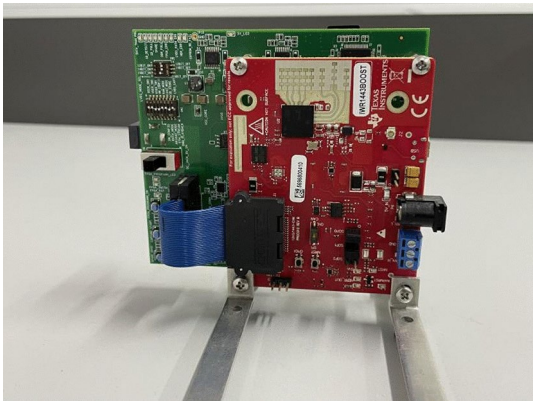

Fig. 10. Hardware connection.

Parameter	Numerical value
Start frequency/GHz	77
FM slope/(MHz)	65.998
Signal period/ms	50
Number of fast time dimension sampling points	200
Number of sampling points in slow time dimension	512
Fast time dimensional sampling rate/(MHz·s-1)	5
Bandwidth/(GHz)	3.959

Table 1. Mmwave radar parameter settings.

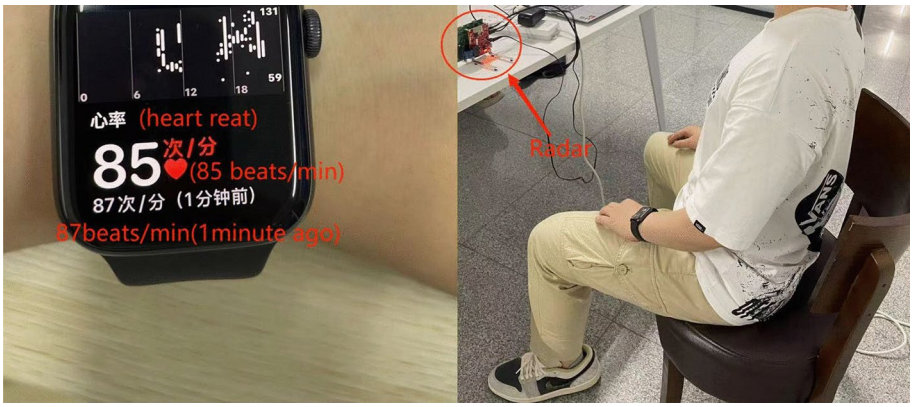

Fig. 11. Scenario diagram of the vital signs acquisition experiment.

Comparative experiments with existing algorithms

The aim of this study is to validate the significant improvement of our proposed method in heart rate detection accuracy compare to the variational modal decomposition algorithm. Additionally, we aim to ensure the accuracy of the experimental data. We replicate the experimental scenario described in[28] to the best of our ability. In this scenario, the experimenter sits directly in front of the radar sensor in an open area. The experimenter stands approximately 0.65 meters away from the radar, as shown in Fig 11. To obtain reliable reference heart rate data, the experimenter wears an Apple Watch to measure heart rate during the experiment. During the experiment, the experimenter is instructed to maintain an upright and stationary position until the radar indicator stops flashing. Since the Apple Watch displays heart rate data as the number of heartbeats per minute, we are providing a conversion formula between heart rate and heartbeats to make the experimental results more intuitive and easier to understand.

$$hr_{mlen} = f_h \times 60. \tag{26}$$

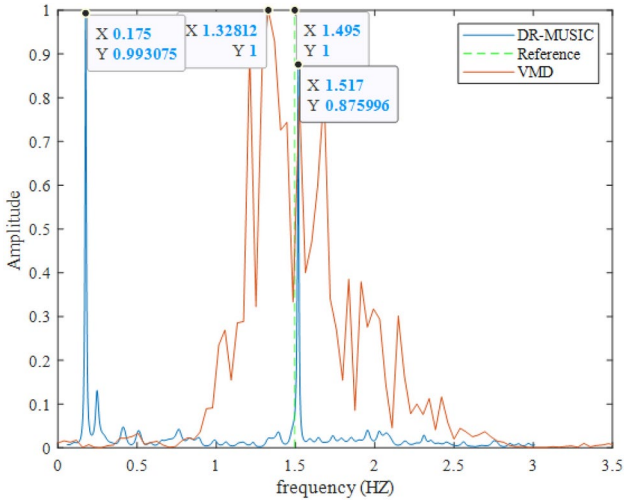

Fig. 12. Comparison of spectrograms generated by different algorithms.

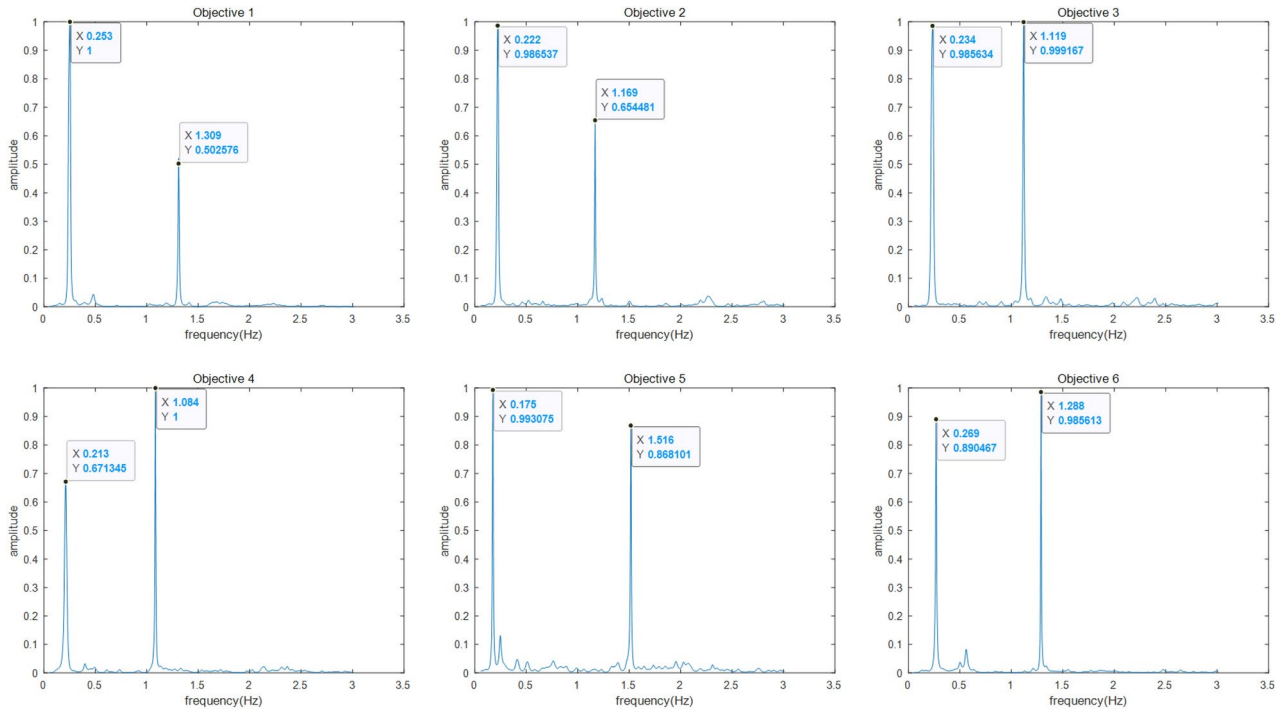

Fig. 13. Results of the spectrogram for various experimenters.

where f_h represents the heartbeat frequency and hr_{mlen} represents the number of heartbeats measured.

Figure 12 clearly displays the spectrogram of heart rate estimation obtained after using two different algorithms. The respiratory signal corresponds to a frequency of 0.175 Hz. The VMD algorithm yields a heartbeat signal frequency of 1.32 Hz, while the reference value is 1.495 Hz. Finally, the frequency of 1.517 Hz corresponds to the heartbeat signal processe by our proposed DR-MUSIC algorithm. The frequencies correspond to 80, 90, and 91 heartbeats per minute, respectively, according to the conversion of Equation 25. The figure shows that our proposed DR-MUSIC algorithm provides heart rate estimates that are very close to the actual reference value, with an error of only one heartbeat per minute. The experimental results indicate that the DR-MUSIC algorithm is more accurate than the VMD algorithm in estimating heart rate.

Single target multiple-measurement experiments

To improve the reliability and accuracy of the DR-MUSIC algorithm in single-target scenarios, we conduct multiple measurement experiments. Six experimenters sat in a resting state directly in front of the millimeter-

Subject	Age	BMI	X_1/C_1	X_2/C_2	X_3/C_3	X_4/C_4	X_5/C_5	X_6/C_6	η
1	24	28.0	80/79	76/79	77/79	81/80	80/79	79/78	1.89%
2	23	19.1	73/70	73/76	71/70	68/66	73/72	69/70	2.57%
3	25	25.6	69/71	70/72	74/72	67/66	69/67	70/69	2.35%
4	24	31.2	68/65	68/66	65/66	70/71	63/60	67/65	2.43%
5	26	21.8	88/91	86/88	90/89	89/87	88/88	92/90	1.69%
6	23	23.8	79/76	78/79	77/78	76/74	74/73	80/76	2.61%

Table 2. Results of heartbeat estimation by different experimenters.

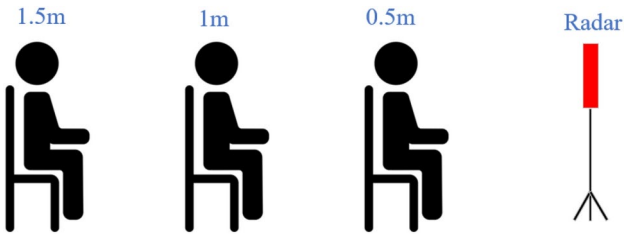

Fig. 14. Heart rate measurement scenarios at various distances.

Range	Age	BMI	η
0.5m	26	22.6	1.61%
1m	25	24.3	1.82%
1.5m	25	23.8	2.01%

Table 3. Heart rate error results at different distances.

wave radar sensor at a distance of 0.65 meters. The radar sensor collected thoracic vibration echo signals for a duration of 51.2 seconds, and the heart rate values measured by the Apple Watch were used as the reference standard for each experiment. To eliminate randomness, each experimenter performed six experiments under the same conditions. We evaluate the performance of the DR-MUSIC algorithm more comprehensively by comparing the error between the heart rate values measured in each experiment and the reference value. To present the experimental results objectively, average error rate is calculated using the following formula:

$$\eta = \frac{1}{N}\left(\frac{\sum_{i=1}^{N} \mid X_i - C_i \mid}{\sum_{i=1}^{N} C_i}\right) \times 100\%. \tag{27}$$

Where: X_i represents the estimated heart rate value, C_i represents the reference heart rate value and η represents the mean error rate.

As shown in Fig 13. it is evident that the spectrograms maintain the frequencies of respiratory and heartbeat signals, suppress respiratory harmonics, and significantly amplify the amplitude of heartbeat signals.

Tab 2 displays a slight discrepancy between the estimated heart rate and the reference heart rate, with an error range of 1.69% to 2.61%. This error rate is approximately 8.1% lower than the error rate reported in[28] for the same experimental environment. These results confirm the viability of the vital signs detection method proposed in this paper.

Heart rate measurement accuracy at various distances

This subsection investigates the effect of distance conditions on the accuracy of heart rate detection. The experimenter collects chest echo data from the radar sensor at three different positions: 0.5 m, 1 m, and 1.5 m. The reference heart rate is measured using the Apple Watch, as shown in Fig 14. Tab 3 presents the experimental results, which demonstrate that our algorithm can achieves a heart rate detection accuracy of 98% or higher at a distance of 1.5 meters.

Conclusion

This paper presents a method for estimating heart rate using mmWave radar that addresses key challenges encountered by traditional methods. To eliminate baseline drift caused by human body micromotion, we use median filtering. We propose the DR-MUSIC algorithm to address the interference of respiratory harmonics

on heartbeat signals. The reliability and efficiency of the algorithm are verified through numerous experiments. To implement the algorithm, we first use the RLS adaptive noise cancellation method to suppress respiratory harmonics. Then, we amplify the amplitude of the heartbeat signal through differential operations. Finally, we use the MUSIC algorithm to obtain highly accurate spectrograms, which allows us to accurately estimate the heart rate. MATLAB simulation experiments are conducted to demonstrate the superior performance of the DR-MUSIC algorithm in suppressing respiratory harmonics and enhancing heartbeat signals. The mmWave radar measurements show that the algorithm accurately estimates the heart rate and significantly improves the accuracy compared to the traditional VMD algorithm. We verify the validity and feasibility of the scheme through several single-target measurement experiments and heart rate accuracy measurements at different distances, while excluding random factors. The success of this work not only enhances the utility of non-contact vital sign detection technology but also lays the groundwork for its expansion into a wider range of applications. Future research directions include multiple vital signs detection, implementing real-time algorithms, and porting to mmWave radar chips to improve performance and application breadth.

Data availability

The datasets generated and/or analyzed during the current study are not publicly available due to confidentiality agreements but are available from the corresponding author on reasonable request.

Received: 6 May 2024; Accepted: 24 October 2024
Published online: 26 October 2024

References

1. Acharya, U. R., Joseph, K. P., Kannathal, N., Lim, C. M. & Suri, J. S. Heart rate variability: A review. *Med. Biol. Eng. Comput.* **44**(12), 1031–1051. https://doi.org/10.1007/s11517-006-0119-0 (2006).
2. Avram, R. et al. Real-world heart rate norms in the health eHeart study. *NPJ Digit. Med.* **2**(1), 1–10. https://doi.org/10.1038/s41746-019-0134-9 (2019).
3. Weissler, A. M., Peeler, R. G. & Roehll, W. H. Relationships betweenleft ventricular ejection time, stroke volume, and heart rate in nor-mal individuals and patients with cardiovascular disease. *Amer. HeartJ.* **62**(3), 367–378. https://doi.org/10.1016/0002-8703(61)90403-3 (1961).
4. Zhang, Z. Photoplethysmography-Based Heart Rate Monitoring in Physical Activities via Joint Sparse Spectrum Reconstruction. *IEEE Trans. Biomed. Eng.* **62**(8), 1902–1910. https://doi.org/10.1109/TBME.2015.2406332 (2015).
5. Zijlmans, M., Flanagan, D. & Gotman, J. Heart rate changes and ECG abnormalities during epileptic seizures: prevalence and definition of an objective clinical sign. *Epilepsia.* **43**(8), 1847–1854. https://doi.org/10.1046/j.1528-1157.2002.37801.x (2002).
6. Chen, K.-M., Huang, Y., Zhang, J. & Norman, A. Microwave life-detection systems for searching human subjects under earthquake rubble or behind barrier. *IEEE Trans. Biomed. Eng.* **47**(1), 105–114. https://doi.org/10.1109/10.817625 (2000).
7. Forouzanfar, M. et al. Event Recognition for Contactless Activity Monitoring Using Phase-Modulated Continuous Wave Radar. *IEEE Trans. Biomed. Eng.* **64**(2), 479–491. https://doi.org/10.1109/TBME.2016.2566619 (2017).
8. JalaliBidgoli, F., Moghadami, S. & Ardalan, S. A Compact Portable Microwave Life-Detection Device for Finding Survivors. *IEEE Embedded Sys. Lett.* **8**(1), 10–13. https://doi.org/10.1109/LES.2015.2489209 (2016).
9. Kebe, M., Gadhafi, R., Mohammad, B., Sanduleanu, M., Saleh, H., & A1-Qutayri, M. Human Vital Signs Detection Methods and Potential Using Radars. *A Rev. Sens.* **20**(5), 1454. https://doi.org/10.3390/s20051454 (2020).
10. Luo, Z., Liao, Y. & Xing, M. Target Indication With FMCW-OAM Radar. *IEEE Geosci. Remote Sens. Lett.* **20**, 1–5. https://doi.org/10.1109/LGRS.2023.3314459 (2023).
11. Choi, H.-I., Song, W.-J., Song, H. & Shin, H.-C. Selecting Target Range with Accurate Vital Sign Using Spatial Phase Coherency of FMCW Radar. *Appl. Sci.* **11**(10), 4514. https://doi.org/10.3390/app11104514 (2021).
12. Choi, H.-I., Song, H. & Shin, H.-C. Target Range Selection of FMCW Radar for Accurate Vital Information Extraction. *IEEE Access.* **9**, 1261–1270. https://doi.org/10.1109/ACCESS.2020.3043013 (2021).
13. Alizadeh, M., Shaker, G., Almeida, J. C. M. D., Morita, P. P. & Safavi-Naeini, S. Remote Monitoring of Human Vital Signs Using mm-Wave FMCW Radar. *IEEE Access.* **7**, 54958–54968. https://doi.org/10.1109/ACCESS.2019.2912956 (2019).
14. Anghel, A., Vasile, G., Cacoveanu, R., Ioana, C. & Ciochina, S. Short-Range Wideband FMCW Radar for Millimetric Displacement Measurements. *IEEE Trans. Geosci. Remote Sens.* **52**(9), 5633–5642. https://doi.org/10.1109/TGRS.2013.2291573 (2014).
15. Chicco, F., Rengifo, S. C., Pengg, F. X., Le Roux, E. & Enz, C. Power-Optimized Digitally Controlled Oscillator in 28-nm CMOS for Low-Power FMCW Radars. *IEEE Microwave Wireless Compon. Lett.* **31**(8), 965–968. https://doi.org/10.1109/LMWC.2021.3092182 (2021).
16. Lee, H., Kim, B.-H., Park, J.-K., Kim, S. W. & Yook, J.-G. A Resolution Enhancement Technique for Remote Monitoring of the Vital Signs of Multiple Subjects Using a 24 Ghz Bandwidth-Limited FMCW Radar. *IEEE Access.* **8**, 1240–1248. https://doi.org/10.1109/ACCESS.2019.2961130 (2020).
17. Abedi, H. et al. AI-Powered Noncontact In-Home Gait Monitoring and Activity Recognition System Based on mm-Wave FMCW Radar and Cloud Computing. *IEEE Internet Things J.* **10**(11), 9465–9481. https://doi.org/10.1109/JIOT.2023.3235268 (2023).
18. Huang, X., Sun, L., Tian, T., Huang, Z., & Clancy, E. Real-time non-contact infant respiratory monitoring using UWB radar. in *Proc. IEEE 16th Int. Conf. Commun. Technol,* Hangzhou, China. 493-496. https://doi.org/10.1109/ICCT.2015.7399885 (2015).
19. Schmiech, D., Muller, S., & Diewald, A. R. 4-Channel I/Q-Radar System For Vital Sign Monitoring In A Baby Incubator. in *Proc. 19th Int. RadarSymp,* Bonn, Germany, 1-9. https://doi.org/10.23919/IRS.2018.8448163 (2018).
20. Li, C. et al. A Review on Recent Progress of Portable Short-Range Noncontact Microwave Radar Systems. *IEEE Trans. Microwave Theory Tech.* **65**(5), 1692–1706. https://doi.org/10.1109/TMTT.2017.2650911 (2017).
21. Lin, J., & Wu, W. Vital sign radars: Past, present, and future. in *Proc.WAMICON,* Tampa, FL, USA, 1-4. https://doi.org/10.1109/WAMICON.2014.6857798 (2014).
22. Li, C., & Lin, J. Complex signal demodulation and random body move-ment cancellation techniques for non-contact vital sign detection. in *IEEE MTT-S Int.Microw. Symp. Dig,* Atlanta, GA, USA, 567-570. https://doi.org/10.1109/MWSYM.2008.4633229 (2008).
23. Li, C., Lin, J., & Xiao, Y. Robust Overnight Monitoring of Human Vital Signs by a Non-contact Respiration and Heartbeat Detector. in *Proc. Int.Conf.IEEE Eng. Med. Biol. Soc.,* New York, NY, USA, 2235-2238. https://doi.org/10.1109/IEMBS.2006.260148 (2006).
24. Tu, J., & Lin, J. Respiration harmonics cancellation for Accurate Heart Rate measurement in non-contact vital sign detection. in *IEEE MTT-S Int.Microw. Symp. Dig,* Seattle, WA, USA, 1-3. https://doi.org/10.1109/MWSYM.2013.6697732 (2013).
25. Huang, T.-Y., Hayward, L., & Lin, J. Adaptive harmonics comb notch digital filter for measuring heart rate of laboratory rat using a 60-GHz radar. in *IEEE MTT-S IMS,* San Francisco, CA, USA, 1-4. https://doi.org/10.1109/MWSYM.2016.7540004 (2016).

26. Tu, J. & Lin, J. Fast Acquisition of Heart Rate in Noncontact Vital Sign Radar Measurement Using Time-Window-Variation Technique. *IEEE Trans. Instrum. Meas.* **65**(1), 112–122. https://doi.org/10.1109/TIM.2015.2479103 (2016).
27. Hu, W., Zhao, Z., Wang, Y., Zhang, H. & Lin, F. Noncontact Accurate Measurement of Cardiopulmonary Activity Using a Compact Quadrature Doppler Radar Sensor. *IEEE Trans. Biomed. Eng.* **61**(3), 725–735. https://doi.org/10.1109/TBME.2013.2288319 (2014).
28. Duan, Z. & Liang, J. Non-Contact Detection of Vital Signs Using a UWB Radar Sensor. *IEEE ACCESS.* **7**, 36888–36895. https://doi.org/10.1109/ACCESS.2018.2886825 (2019).
29. Ling, Z., Zhou, W., Ren, Y., Wang, J. & Guo, L. Non-Contact Heart Rate Monitoring Based on Millimeter Wave Radar. *IEEE ACCESS.* **10**, 74033–74044. https://doi.org/10.1109/ACCESS.2022.3190355 (2022).
30. Muller, M., Ellis, D. P. W., Klapuri, A. & Richard, G. Signal Processing for Music Analysis. *IEEE J. Sel. Top. Signal Process.* **5**(6), 1088–1110. https://doi.org/10.1109/JSTSP.2011.2112333 (2011).

Author contributions

Y.C. conceived the concept and study design, collected the data, and performed the data preprocessing. J.Y. developed the algorithm for analyzing the data. Y.C. analyzed the data, visualized the results, and wrote the paper. J.Y. received research funding. J.Y. and J.T. supervised the project. All authors contributed to the interpretation of the results and approved the final manuscript.

Declarations

Competing interests

The authors declare no competing interests.

Additional information

Correspondence and requests for materials should be addressed to J.Y.

Reprints and permissions information is available at www.nature.com/reprints.

Publisher's note Springer Nature remains neutral with regard to jurisdictional claims in published maps and institutional affiliations.